Anal. Chem. **XXXX,** *xxx,* 000–000

analytical chemistry
feature

Synchrotron IR Spectromicroscopy: Chemistry of Living Cells

Hoi-Ying N. Holman, Hans A. Bechtel, Zhao Hao, and Michael C. Martin

Lawrence Berkeley National Laboratory

Advanced analytical capabilities of synchrotron IR spectromicroscopy meet the demands of modern biological research for studying molecular reactions in individual living cells. (To listen to a podcast about this article, please go to the Analytical Chemistry multimedia page at pubs.acs.org/page/ancham/audio/index.html.)

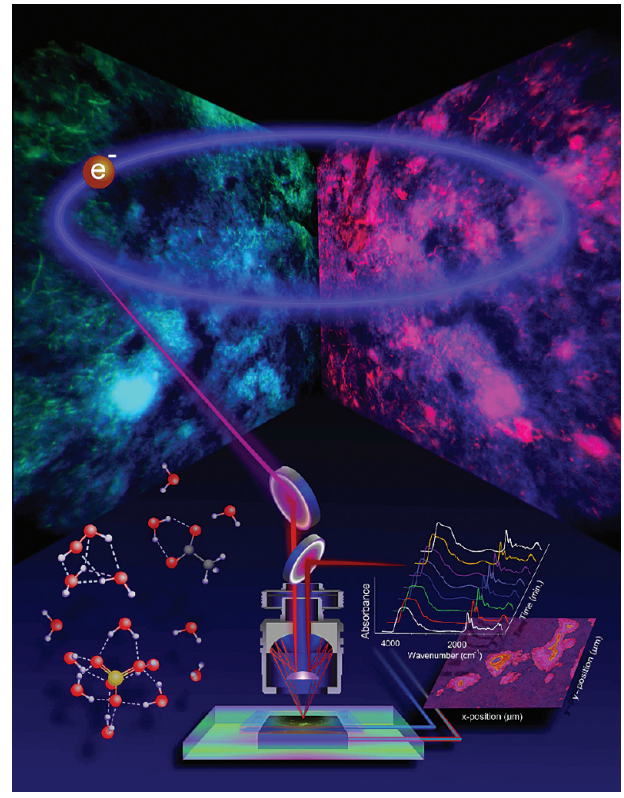

ROBERT GATES

The ability to modify cellular processes in response to changes in internal or external environment is critical for maintaining an efficient functional state in living cells. Much of our quantitative understanding of cellular molecular reactions has come from traditional biochemistry experiments that are either averaged over large populations or performed *in vitro* with purified biomolecules. Although these approaches have clarified many detailed mechanisms, they are not sufficient to reveal the phenotypic differences that exist even within a genetically homogeneous population. These phenotypic variations are important in fields ranging from ecology to pathogenesis[1−3] and may arise from population heterogeneities in cell cycle phase, cell ageing, epigenetic regulation,[4] or infrequently and transiently expressed maintenance genes[5] or stochastic gene switching.[6] Furthermore, recent advances in sequencing and functional metagenomic and metaproteomic profiling have yielded cellular genetic "blueprints", revealing complex networks of regulatory and metabolic processes. The chemical reaction components of these networks in living cells may exhibit both spatial and temporal separation—and are therefore difficult to simulate in non-biological *in vitro* systems.

The challenge is to identify those cells of ecological or medical importance within a large population and track their biochemical reactions *in situ* in real time. In this article, we highlight advances that now allow IR spectromicroscopy to address this challenge. Central to these advances is the synchrotron light source, which enables high-throughput noninvasive spectroscopic microanalysis. This capability can precisely target subpopulations with diffraction-limited spatial resolution and accuracy to track their chemical reactions with high molecular specificity without the use of labels—all at timescales that are associated with important biological processes.

THE IR APPROACH

Mid-IR region spectroscopy (~2.5−15.5 μm wavelength, or ~4000−650 cm^{-1} wavenumber) is powerful and nondestructive and provides label-free fingerprint-like spectra originating from the characteristic vibrational frequencies of various chemical bonds and, therefore, functional groups.[7] IR spectroscopy provides a wealth of chemical information about the sample without *a priori* knowledge and has excellent sensitivity to hydrogen bonding. Changes in hydrogen bond lengths and

10.1021/ac100991d

angles of as little as 0.01 Å or 1°, respectively, can provide clear differences in a vibrational spectrum.[8] This specificity and sensitivity makes the technique an excellent tool for studying the structure and function of biological macromolecules, which both affect and are affected by their immediate hydrogen bonding environment.

The application of IR spectroscopy to the study of biological tissues and cells began >60 years ago when two research groups reported using a reflecting microscope with mid-IR light to obtain detailed molecular information in biological specimens.[9,10] They demonstrated that even though an IR spectrum is a sum of the contributions gathered from all biomolecules (i.e., proteins, amino acids, lipids, and nucleic acids), distinct absorption bands exist that can be related to known chemical groups in biomolecules. This idea was soon applied by many others to investigate the chemical composition of biological samples in the absence of distinctive morphological features.[11−13] In spite of the apparent simplicity of this IR spectroscopy-based microscopy method and the extensive characterization of spectral fingerprints representative of biological macromolecules, the approach remained uncommon, while fluorescence microscopy became the popular method for studying live cellular processes such as the dynamics of gene expressions. Following Digilab's pioneer work in FTIR instrumentation in 1970s, IR spectroscopy-based microscopy rose again in the 1990s with the improved speed and sensitivity of fast FTIR spectromicroscopy (also called microspectroscopy). An excellent summary of the theory and practice of FTIR spectromicroscopy can be found in an article by Bhargava and Levin.[14] Subsequent improvements in instrumentation and data evaluation methods (aided by the availability of low-cost, high-speed computers) led to the robust and reliable use of FTIR spectromicroscopy to study the chemical composition and structure of complex biological samples from a range of biological systems including microorganisms, plants, animals, and humans.[15]

Improvements in two technical parameters have had significant implications for FTIR spectromicroscopy studies of tissues, intact cells, and microorganisms: 1) spatial resolution, which determines the measurement area within the biological sample and therefore the length scale of the heterogeneity that can be studied and 2) detection sensitivity, which determines the data collection time and therefore time resolution for investigating ongoing biological processes in real time. Both these parameters can be significantly improved by replacing the thermal emission source (e.g., a globar) in the conventional FTIR spectromicroscope with a bright synchrotron IR source.[16,17]

THE BRILLIANCE OF SYNCHROTRON IR

A synchrotron is a high-energy electron storage ring optimized for the production and collection of light radiated by relativistic electrons as they traverse a curved path through a magnetic field. Synchrotron radiation (SR) spans a large electromagnetic spectral range, beginning in the far-IR and extending through much of the X-ray region. The synchrotron IR is 100−1000× brighter than a conventional thermal IR source because the SR is concentrated in a very small opening angle such that the effective source size can be very close to an ideal point source.[16] Interested readers are directed to an informative overview of SR by Sham and Rivers.[18] When coupled to an IR microscope (Figure 1a), the greater brightness of synchrotron IR light means that the photons

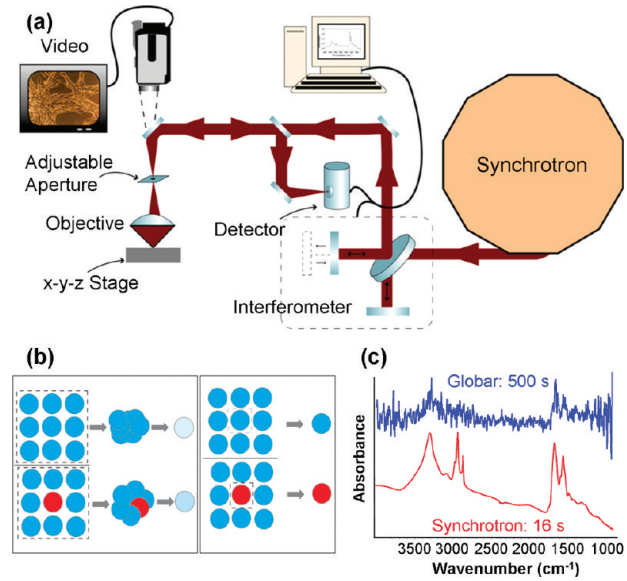

Figure 1. Basics of SR-FTIR. (a) Schematic of an SR-FTIR spectromicroscopy experiment, in which the thermal source of a conventional FTIR microscope is replaced by a synchrotron source. Mid-IR radiation from a synchrotron is transported to an FTIR interferometer bench. After modulation by the interferometer, an IR microscope with reflective optics focuses the beam onto the sample. The stage is computer controlled and rasters the sample in the $x-y$ plane with 0.1 μm precision to obtain spectral maps across the sample. (b) Demonstration of how improved spatial resolution can enhance detection sensitivity and spatial accuracy of heterogeneous samples within a larger population. The left panel demonstrates that with a larger spot size (from a poor brilliance source such as a conventional thermal emission source), the abnormal (red) circle is averaged with the normal (blue) circles and can be hidden. In the right panel, the smaller spot size (from a high brilliance source such as a synchrotron), the abnormal circle is clearly identified (adapted with permission from ref. 17; copyright Elsevier). (c) Comparison of FTIR spectra of a single cell using a 6 × 6 μm^2 aperture from a synchrotron source (red trace) and a thermal (blue trace) source. The collection time for the synchrotron source system was ~16 s (32 scans) compared to ~500 s (1000 scans) for the thermal source system (courtesy of P. Dumas).

can be focused to a diffraction-limited spot that is dependent on the numerical aperture (NA) of the microscope objective and the wavelength (λ) of light. Typical IR microscopes use Schwarzschild objectives with NA in the range of 0.4−0.7, and spot sizes (and hence spatial resolutions) of 0.5−1.2 λ are achievable,[16,19] depending on definition, optical coupling, and synchrotron facility parameters.

The size of the individual cells relative to the size of the SR IR beam is important in biological investigations. In the mid-IR region, these 0.5−1.2 λ (i.e., ~2−10 μm) diffraction-limited spot sizes are smaller than eukaryote cells, are larger than most of the prokaryotes and archaea (except for a few mega-bacteria such as the sulfur bacterium *Thiomargarita namibiensis* that can reach a diameter of 700 μm or the thermophilic archaea *Staphylothemus marinus* that can grow to 15 μm in diameter), and are comparable to a small cluster of prokaryote or archaea species. Also, with a synchrotron source there is no loss in S/N to obtain a diffraction-limited spot, unlike with a thermal source that must use apertures to achieve micrometer spatial precision and resolution. Although many more IR photons are focused on the biological sample when using a synchrotron source than when using a conventional globar

source, the low photon energy and low peak powers (relative to the alternative IR laser sources) of <~50 mW have shown no detectable effects on living cells.[20]

This improved spatial resolution and S/N achievable with synchrotron IR light are of great benefit to measurements involving heterogeneous samples, such as tissues or communities of microbes. As illustrated in Figure 1b, the measurement is targeted to a small area, more accurately pinpointing which a part of the sample gives rise to a feature of interest.[17] In Figure 1c, the improvement in S/N and time resolution of SR-FTIR is demonstrated by comparing FTIR spectra from a single cell, as measured with a synchrotron and with a conventional thermal source using a 10-μm aperture. In this example, the collection time using the synchrotron source was only 16 s (32 scans) whereas the collection time using the thermal source was 500 s (1000 scans). Even after extensive averaging, the quality of the thermal source measurement is not sufficient to reveal the fine molecular features within the vibrational spectrum. Indeed, prior to the incorporation of synchrotron light, the low S/N made it exceptionally difficult to apply conventional IR spectroscopy to follow the dynamics of cellular processes.

The high SR IR brightness coupled with its noninvasive nature has already made a significant impact in the fields of biomedicine,[21] environmental ecology, and geochemistry.[22] In an early study from our group, time-lapse SR-FTIR reflectance measurements showed the mechanism by which a small subset of microbes on a basalt rock specimen survived exposure to a high concentration of toxic chromium(VI) when most of the surrounding microbial cells were killed.[23] Although geological materials inherently have very rough surfaces, the small spot size of the SR IR source allowed us to measure a small region containing a handful of microorganisms, revealing that they were reducing chromium(VI) to chromium(III). This capability of SR-FTIR also yielded new insights into how the soil bacteria *Mycobacterium* sp. JLS solubilize large recalcitrant organic pollutants such as polycyclic aromatic hydrocarbons and metabolize them into biomass.[24] This understanding of the dynamic microbial processes in simulated geological environments has contributed to the design of environmental cleanup strategies.

WATER: THE GOLDILOCKS PROBLEM (GETTING IT JUST RIGHT)

Water presents one of the primary challenges of using IR spectroscopy in studying living cells, even with the bright synchrotron source. Water strongly absorbs mid-IR light and even the absorption due to a thin layer of water can completely dominate the spectrum. However, water is necessary for life and is the most common ingredient (>70%) in living cells. So it is essential to get the optical thickness of water "just right": enough to support life and ensure the validity of model systems, but not so much that it masks the molecular signatures of interest. Typically, <10 μm of bulk water is preferred to exploit the molecular information across the full mid-IR spectral range. Historically, most applications of real-time synchrotron IR spectromicroscopy to the study of cellular processes in living cells were limited to hydrated microbial systems maintained in moist microchambers[23−25] or experiments using isotope labeled compounds.[26,27]

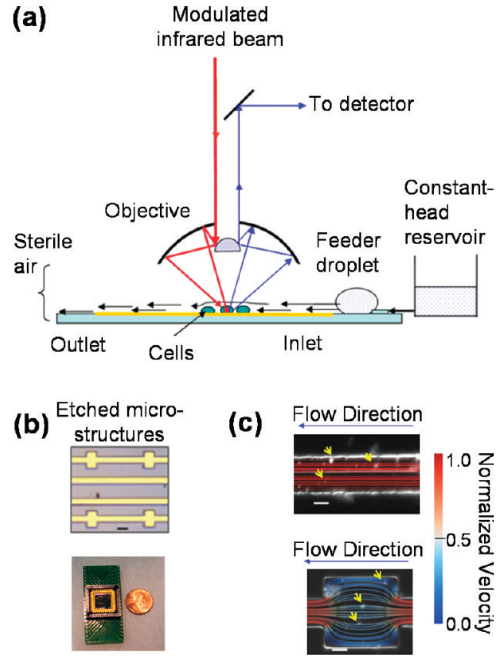

Figure 2. Microfluidic platform to minimize water absorption. (a) Microfluidic SR-FTIR microscopy platform design and setup. (b) Plane view depiction of an example chip with several parallel etched microstructures for multiple simultaneous experiments. (c) Flow maps of the microstructures, simulated from experimentally measured paths of near-neutral density polystyrene beads (yellow arrows) and superimposed on a snapshot image. Top: flow in a microchannel. Bottom: flow in a microwell. Scale bars = 10 μm. Velocity = ~60 μm s^{-1} (adapted from ref. 32).

A traditional approach to minimize water absorption during living cell experiments is attenuated total reflectance (ATR) FTIR equipped with a flow chamber. In ATR FTIR, the IR beam internally reflects off a high index crystal (e.g., diamond or germanium), and the attenuation of the IR beam caused by the absorption of the evanescent wave is measured and analyzed.[28] For living cell experiments, cells are cultured on ATR crystals in a specially designed flow chamber that can carefully control the culturing/experimental conditions (pH, temperature, ionic strength, flow shear stress, and delivery of materials such as nutrients and drugs) for hours.[29−31] The evanescent field formed at the cell/ATR crystal interface has a typical penetration depth of <1 μm, thereby reducing the optical path length in water. However, this small penetration depth, though important in reducing the path length through water, prevents the ATR FTIR technique from examining chemical and biological processes in cells within biological systems with an extensive extracellular matrix. Another important consideration is the effect of growing the cells on the ATR crystal. Many cells require a substratum for normal growth, and the use of an ATR crystal may affect extracellular matrix properties that are important in cellular phenotype. This penetration-depth limitation makes it less than ideal for use in studies of the resistance of bacterial biofilms to antibiotics, the resistance of lung cancer cells to chemotherapy, or the directional movement and proliferation of colon cancer during metastasis.

We used a more straightforward microfluidic approach instead.[32] Figure 2 shows an early version of our open-channel microfluidic device. It was fabricated on a silicon chip using deep reactive ion etching to create hydrophilic microstructures 10−15

μm deep and at least 40 μm wide. A continuous thin-film (<10 μm) laminar flow is maintained by balancing the hydrostatic pressure in a microliter-sized feeder droplet at the microchannel inlet with the capillary forces present at the outlet. In this setup, the bulk flow rate in the open microchannel is typically ~60 μm s^{-1} and is controlled by adjusting the elevation of the off-chip reservoir that supplies the feeder droplet. Mid-IR photons emitted from the synchrotron are focused onto the targeted areas within the microstructures, and SR-FTIR measurements are made by the transflection or transmission modes. To image the biochemical properties and the distribution of bacterial activity across a biofilm, it is raster scanned with equal micrometer-sized steps, collecting a full SR-FTIR spectrum at each position. The ability of the platform to provide a sustainable environment for SR-FTIR measurements of living bacteria has been confirmed by using the reporter bacterium *E. coli* XL1-Blue.

Several other groups have reported uncomplicated flow chamber techniques.[33,34] They commonly placed living cells between two parallel IR transparent windows (e.g., CaF_2) that are separated by a spacer of <12 μm to minimize the aqueous media absorption. Most recently, a more sophisticated closed-chamber microfluidic device has been fabricated by etching channels and wells into two CaF_2 crystals.[35] Although effective in its simplicity, we found that the spectra from closed-chamber or closed-channel devices are often marred by complicated sinusoidal patterns of interference fringes that probably arise from interference between multiple reflections from the parallel surfaces. In our device, the sloping free interface between water and air, which is produced by balancing the hydrostatic pressure in a microliter-size feeder droplet at the microchannel inlet with the capillary forces present at the outlet, has allowed us to completely eliminate the interference fringes during FTIR measurements.

THE RIDDLES OF BACTERIAL BIOFILMS

How do bacteria in biofilms survive antibiotics that should kill them? A bacterial biofilm is a population of cells growing on a surface and enclosed in a self-produced polymeric matrix in an aqueous environment. Bacteria within a biofilm can become up to 1000× more resistant to antibiotics than free-floating bacteria of the same species,[36] yet only ~1% of their genes show differential expression between these two populations.[37]

Figures 3a–c show a dramatic example of using open-channel microfluidics with SR-FTIR spectromicroscopy to study why the antimicrobial agent mitomycin-C (MMC) does not kill some *E. coli* in biofilms.[32] MMC is activated only after it has entered a cell, where it is reduced to a hydroquinone form that covalently cross-links to guanine residues in DNA to form DNA–MMC adducts.[38] The presence of DNA–MMC adduct signals at ~986 cm^{-1} reflects cellular uptake and action of MMC.[32] Figure 3b shows chemical images before and after the introduction of MMC into the microfluidic system. Despite an uninterrupted supply of MMC-laden water, the SR-FTIR image plot shows that MMC uptake is highly localized. DNA–MMC adduct signals are especially strong in areas that were either closer to the MMC source (circles 1 and 2) or in areas formerly rich in protein amide III (~1310 cm^{-1}). In areas with little DNA–MMC adduct, the protein amide III signal increased with MMC exposure. Shown

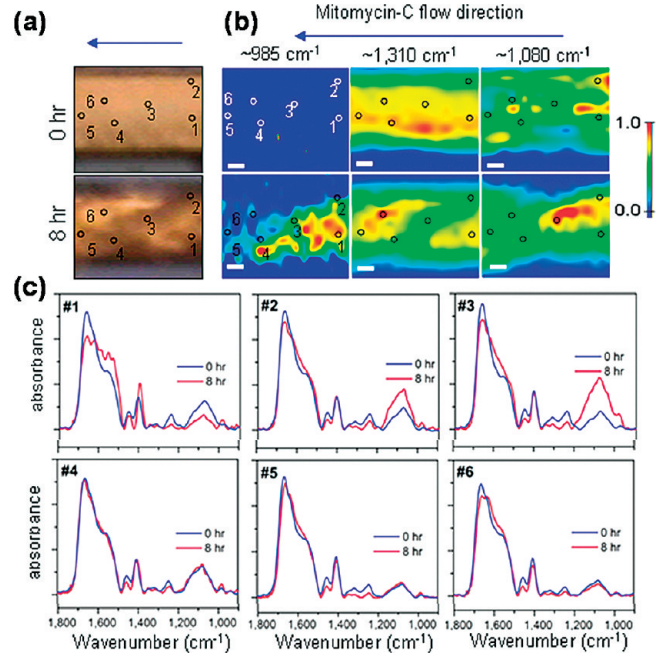

Figure 3. Interactions of antibiotics with *E. coli*. (a) Bright-field optical images of the 1 day old *E. coli* biofilm before (0 h) and during (8 h) 0.15 μg mL^{-1} concentration MMC exposure. (b) SR-FTIR chemical image plots of the intensity before (upper panels) and during (lower panels) MMC exposure at ~985 cm^{-1} (DNA–MMC adducts), ~1310 cm^{-1} (protein amide III), and ~1080 cm^{-1} (polysaccharides). Three distinct biochemical regions formed during MMC treatment: a high MMC-uptake and a low MMC-uptake region separated by an area of high polysaccharide content. Arrows indicate MMC stream direction. Circles in panels mark selected locations. Scale bars = 10 μm. (c) Preprocessed SR-FTIR spectra at selected locations before (blue) and during (red) MMC exposure (adapted from ref. 32).

in Figure 3c are analyses of vector-normalized SR-FTIR spectra (over the 900–1800 cm^{-1} region) at different locations; they also indicate localized small (~10–20 μm) spatial-scale changes in biochemical contents consequent to MMC exposure. We speculate that the localization of MMC may be caused by flow heterogeneities inside the biofilms, perhaps related to internal flow diversions around regions with higher protein amide III signal. The heterogeneous spectral features and behavior, however, may also reflect localized cellular diversification processes in response to MMC toxicity, such as metabolic modification and/or migration to more favorable living areas.

Bacterial real estate: sustainable or a bubble? Our group also used the open-channel SR-FTIR platform to improve the understanding of the growth and development of bacteria on surfaces, a more subtle but growing topic of research interest. Many microbial processes important in pathogenesis and ecology are initiated in microscopic spaces, and recent reports indicate that the colonizing bacterial cells actively seek out confined spaces where biofilm initiation, formation, and evolution could be influenced by fluid dynamics, nutrient supplies, or waste removal.

We compared spectroscopically the dynamics of biofilm formation under two different conditions: in microchannels with higher rates of nutrient supplies and waste product removal and in microwells with lower rates of nutrient supplies and more waste accumulation.[32] Figure 4 shows the remarkable differences. For microchannels of high nutrient supplies and waste removal, four different markers of biofilm formation increase asymptotically:

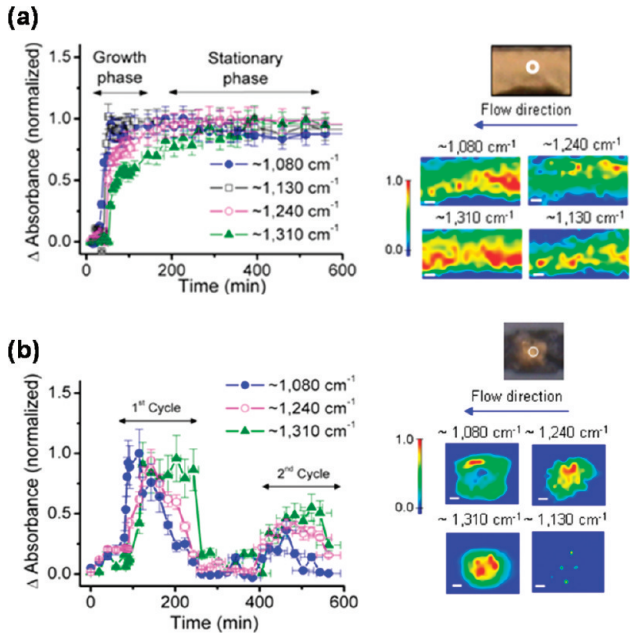

Figure 4. Biofilm dynamics. SR-FTIR time course analyses and chemical images of biofilms (a) in a microchannel and (b) in a microwell (as shown by four molecular markers at ~1080 cm^{-1} (polysaccharides), ~1130 cm^{-1} (glycocalyx), ~1240 cm^{-1} (DNA/RNA polysaccharides), and ~1310 cm^{-1} (protein amide III). Unlike the microchannel data, in which signal intensity of key biomolecules appeared to approach an asymptotic state, the microwell SR-FTIR data were cyclic (cell growth and release). The chemical image plots obtained after the second cycle show locally higher signal intensities of protein amide III and DNA/RNA polysaccharides near the microwell center, whereas the polysaccharide matrix accumulated near the microwell edge. There is little spectroscopic evidence of glycocalyx facilitating strong adherence to the microwell substrate. Scale bars = 10 μm (adapted from ref. 32).

polysaccharide (~1080 cm^{-1}), glycocalyx (~1130 cm^{-1}), DNA/RNA (~1240 cm^{-1}), and protein amide III (~1310 cm^{-1}) (Figure 4a). This result provides chemical evidence that biofilm formation proceeds via multiple convergent genetic pathways. The abundance of glycocalyx carbohydrates in sites with large biofilm growth confirms the belief that glycocalyx synthesis is crucial to the formation of bacterial biofilms.[39] In contrast, biofilm formation in microwells exhibits cyclic growth patterns as indicated by the sequential rise and fall of the different biomolecule signals (Figure 4b). The lack of spectroscopic evidence of glycocalyx suggests that biofilm attachment was weaker in the microwell. A very recent discovery is that some bacteria can produce a factor (mixtures of D-amino acids) that could prevent biofilm formation and cause the breakdown of existing biofilms.[40] Future applications of the SR-FTIR approach to this biological consideration may add a dimension of understanding to the question: why do some bacteria prosper in biofilms whereas others "move away"?

BIOLOGICAL CHEMISTRY AS SEEN BY HYDROGEN BONDS IN CELLULAR WATER

IR sensitivity to structured water molecules constitutes a major advantage of IR spectromicroscopy over other vibrational methods such as Raman spectroscopy methods and enables the detection of chemistry inside living cells. The high sensitivity of IR spectroscopy to the hydrogen bond structure that links cellular water molecules to ions or other small molecules is the key to this new approach, which works well for several reasons. First, >70% of a cell's contents is highly polar water molecules. Second, the hydrogen bond structure of water is a sensitive reflection of the cellular chemical environment because it responds "instantaneously" to ions and other species, such as radicals, small organic acids, and hydrogen gas, which are expected to be present during the functional metabolism of stress adaptive response.[41,42] Furthermore, the IR spectrum of OH stretch vibrations in the hydride−OH dominated stretch region (1900−3800 cm^{-1}) has already been widely used to characterize the dynamics of hydrogen-bonding structures in both water clusters and condensed phases such as aqueous liquids. These studies can be used to guide the interpretation of IR spectra of OH stretch vibrations in the hydride−OH region and to link the variations to the presence of ions and other small molecules in liquid or other condensed phases (for discussion and references, see ref. 44).

Unraveling how descendants of ancient bacteria cope with the stresses of the modern world. We have used SR-FTIR to study how descendents of some of the oldest bacteria can survive oxygen stress from the modern Earth atmosphere. Microbes, such as the ubiquitous sulfate reducing bacteria (SRB), are the oldest (>3.5 billion years) and the smallest (about 1/8000th the volume of a human cell) living organisms on Earth. Strong selection pressure over time and their high surface-to-volume ratio may have enabled these species to cope with many environmental fluctuations. Genome sequencing shows that some SRB descendents have acquired the genetic "blueprints" to survive transiently in an oxygenated atmosphere. This includes the potential capabilities to reduce O_2 and cope with the subsequent toxic reactive oxygen species (ROS) in the modern atmosphere, such as superoxide anion radicals ($O_2^{\bullet -}$), peroxides (H_2O_2), and hydroxyl radicals ($HO^{\bullet}$).

In the case of our model SRB, *Desulfovibrio vulgaris* Hildenborough, only a small number of cells in a population can survive transient exposure to atmospheric oxygen (Figure 5a). These few "survivors" often exist individually or in small groups of several cells to form localized microscopic communities. They must be interrogated without spectroscopic influence from neighboring cells in the population that are dying. We also know from transcriptomics analysis that the time scales of the oxygen adaptive response processes can potentially range from minutes to hours.[43] In order to avoid long data acquisition times and thus capture the response dynamics at shorter time scales, a brilliant IR source providing high S/N is required.

The first step to study the chemistry of adaptive survival response is to identify *a priori* the few survivor cells in the *D. vulgaris* population. Our previous experience shows that only cells that are entering the early stationary phase of the cell cycle and have accumulated an internal reserve of polyglucose and elemental sulfur are likely to survive transient air exposure.[44] The FTIR spectra of polyglucose-accumulated *D. vulgaris* (Figure 5b and c) show the distinct spectral features of the nonglycosidic polyglucose vibration (υC−OH) band between 1055 and 1045 cm^{-1} and the glycosidic linkage vibration (υC−O−C) at ~1175 cm^{-1} (Figure 5b). This spectral information is used to look for the potential survivors in a thin layer of *D. vulgaris* clones that are maintained in an oxygen-free moist atmosphere inside the microscope-stage environmental chamber. By rastering the diffraction-limited synchrotron IR beam across the thin film, one can identify spots where the IR spectrum

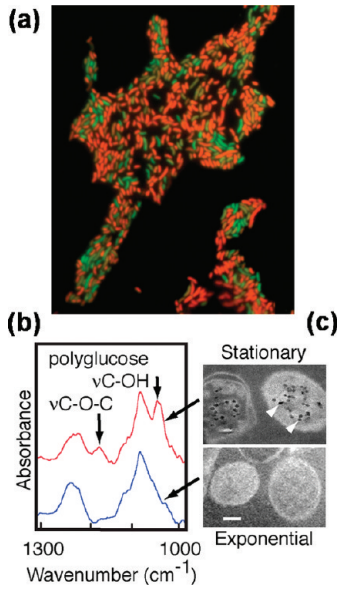

Figure 5. Survivor SRB. (a) Viability of SRB after exposure to moist air for 8 h. Live (green) and dead (red) were assessed using reagents in LIVE/DEAD *Bac*Light Bacterial Viability kit. (b) Typical IR absorption spectra of stationary-phase (red) and exponential-phase (blue) *D. vulgaris* (c) Transmission electron microscopy images of thin sections poststained by the periodic acid thiosemicarbazide-osmium method show intracellular polyglucose granules in stationary-phase but not exponential-phase *D. vulgaris* (adapted with permission from ref. 44, copyright 2009 National Academy of Sciences, U.S.A.).

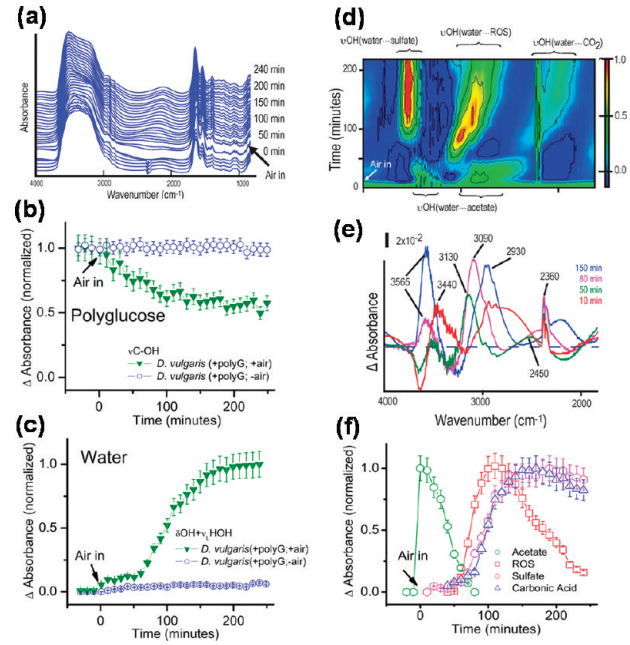

Figure 6. Oxidative stress and adaptation. (a) Typical real-time SR-FTIR spectra of *D. vulgaris* during the transition from an anaerobic to aerobic environment. Sequential spectra are offset upward for clarity. Because all spectra are derived using air as a reference, the abrupt change in the spectral feature at ~2348 cm^{-1} is associated with the presence of atmospheric CO_2. Typical time-course of IR intensity (normalized by the maximum value) of (b) polyglucose content and (c) water. (d) Time versus frequency contour plot of SR-FTIR time-difference spectra in the hydride−OH dominated stretch region. (e) Snapshots of time-difference spectra for selected different time points. The dashed line marks zero difference absorbance. (f) Typical time-course of IR intensity (normalized by the maximum value) of H-bonded species. (Bars: ± 10% error.) (Adapted with permission from ref. 44, copyright 2009 National Academy of Sciences, U.S.A.)

exhibits spectral features similar to the typical IR spectrum of polyglucose-bearing living *D. vulgaris*.

In order to survive oxygen exposure, these polyglucose-bearing bacteria must be metabolically active before exposure. Metabolic activity can be verified by immediately making a short, sequential, uninterrupted series of SR-FTIR measurements. The cells are metabolically active if the analysis of time-difference spectra (derived from the series of real-time spectra) reveals positive time-difference absorption features (bands at ~3190 cm^{-1} and ~3645 cm^{-1} and a shoulder feature at ~3745 cm^{-1}) of water molecules H-bonded with hydrogen gas.[44] Hydrogen gas production is selected as an indicator because it is consistent with the central metabolism of *D. vulgaris* under anaerobic conditions.

The graph in Figure 6a is an overview of the striking molecular changes in *D. vulgaris* survivors during their exposure to atmospheric oxygen. The trends seen in Figure 6b and 6c, which were derived from spectrally integrated absorption intensities of polyglucose and water bands,[44] reveal an unanticipated multiphasic pattern. These two molecules are of immediate interest because the reduction of dioxygen to water through aerobic respiration of internal polyglucose reserves was previously believed to be the primary step in air-tolerant SRB. Comparing trends in these two figures shows that from $0 < t < \sim 50$ min, there is a substantial decrease in the polyglucose band intensity (green inverted triangles in Figure 6b), but little change in the water band intensity (green inverted triangles in Figure 6c). At $t > \sim 50$ min, the water band intensity increases abruptly, whereas the rate of polyglucose disappearance continues unabated until slowing down distinctly later ($t > \sim 100$ min). We elucidate the mechanism(s) underlying this puzzling multiphasic behavior by analyzing the time-difference spectra in the hydride−OH region.[44]

Figure 6d is a 2D time-frequency contour plot of the time-difference spectra (negative values are shown in dark blue), with difference spectrum snapshots beneath (Figure 6e). The contour map reveals the remarkable changing absorption features from υOH as a function of time, which reflects a cascade of chemical reactions (Figure 6f) that sheds light on genetically controlled pathways.[44] A summary of these time-dependent chemical events and their consistency with some known putative events of oxygen-stress adaptive response is highlighted in Figure 7. A comparison indicates that during the initial phase ($t < \sim 50$ min), the cells consume polyglucose (green inverted triangles in Figure 6b) to produce acetate (a two-carbon carboxylate; green circles in Figure 6e) that initially accumulates. Chemical reactions diversify during the intermediate phase ($\sim 50 < t < \sim 150$ min). At $t > \sim 50$ min, the spectra show two dominant types of chemical reactions. (i) Carboxylates (acetate) are converted to CO_2 (compare the green circles for acetate and the blue triangles for CO_2 in Figure 6e), which coincides with increasing water content (see the inverted green triangles in Figure 6c). This coincidence suggests an onset of an ATP generating pathway. (ii) ROS begin to accumulate, signifying that their rate of formation exceeds their removal by protective enzymes and other mechanisms in *D. vulgaris* (red squares in Figure 6e). Then, at $t \approx 70$ min, a striking new spectral feature indicates the formation of sulfate anions, which surprisingly coincides with both the disappearance of ROS (compare the pink

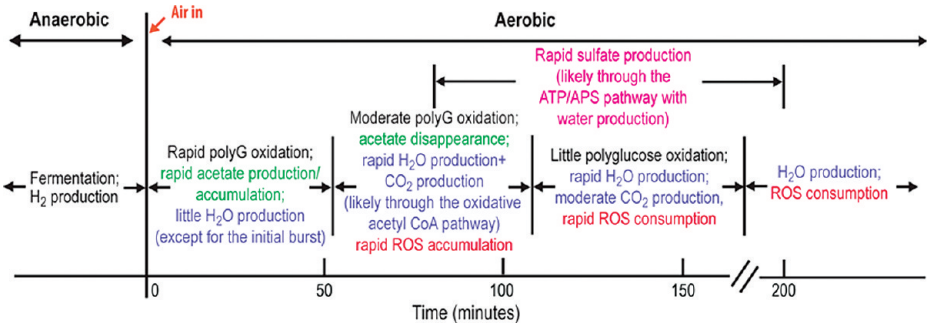

Figure 7. A summary of the evolving cellular chemical environment and possible survival mechanisms inside the same living *D. vulgaris* as in Figure 6 during its transient oxygen-stress and adaptive response, as revealed by SR-FTIR measurements and analyses. Polyglucose is labeled as PolyG; scale bar = 0.5 μm. (Adapted with permission from ref. 44, copyright 2009 National Academy of Sciences, U.S.A.).

hexagons to the red squares in Figure 6e) and an increase of water content (green inverted triangles in Figure 6c). Others have reported that *D. vulgaris* can potentially oxidize its accumulated elemental sulfur and other reduced sulfur compounds and that the oxidation is by means of an ATP/adenyl sulfate pathway that couples the sulfate ion formation with oxygen reduction to water. For longer times ($t > \sim$150 min), the intensity of the υOH band of the water···ROS bond declines (red squares in Figure 6e), which suggests an improved ROS removal rate in the survivor cells.

The mechanisms by which SRB survive transient exposure to atmospheric oxygen have been controversial, partly because of the approach of averaging over a large population. Our SR-FTIR technique provides the first direct molecular observation of the reduction of dioxygen to water by a small number of SRB through aerobic respiration of internal polyglucose reserves as one crucial step and identifies the transient chemical reactions that allow the survivor subpopulation to adapt to extreme changes in its environment.

INTERROGATING SUB-CELLULAR CHEMISTRY IN LARGE LIVING CELLS

As described above, SR-FTIR is an excellent tool for interrogating chemical reactions in living bacterial cells. Many of the techniques described here for studying bacteria may be extended to study subcellular chemical processes in larger cells and tissues. For example, other research groups have used SR-FTIR to probe subcellular chemistry in living cells that are several tens to several hundreds micrometers in size. Jamin et al.[25] first demonstrated the advantage of a synchrotron source by imaging the subcellular components of single intact mammalian cells. After a time, Moss et al. combined SR-FTIR with a flow-through system to examine the growth of single live colorectal cancer cells over several hours.[45] Metabolite formation in living unicellular algae (*Chlamydomonas reinhardtii*) was also recorded over time using recently improved instrumentation technology.[27] In addition, several groups reported the observation of subcellular chemical changes in living cells as the cells responded to environmental changes. For example, Heraud et al. mapped nutrient-induced biochemical changes in living algal cells (*Micrasterias hardyl*) and reported that the largest changes occurred in the chloroplast compartments.[46] The Gough group reported significant chemical changes in fungal hyphae committed to spore development.[47] More recently, researchers in the Dillion group observed arsenic-induced changes in membrane and secondary protein structures in living HL60 cells.[48] Although these examples are frontier breaking, they have only begun to scratch the surface of the potential of SR-FTIR for studying cellular chemistry inside subcompartments of living mammalian cells, plant cells, and many other eukaryotic cells.

PROSPECTS

Synchrotron IR spectromicroscopy shows great potential for studying biochemical reactions in living microbial cells when conventional methods of averaging over a large population are inadequate. The diffraction-limited spot size of synchrotron IR enables us to investigate chemistry in bacteria and archaea and at a subcellular level in cells tens to hundreds of micrometers in size. Examination of the riddles of biofilms and investigation of a stress-adaptive response in live cells of different sizes illustrate that SR-FTIR spectromicroscopy is particularly powerful for systems that cannot be well understood by conventional approaches. From a careful analysis of the real-time multiple-dimension spectra with time resolutions from seconds to days, SR-FTIR spectromicroscopy studies can identify key chemical reactions underpinning phenotypic diversity and individuality in cells within a population, with applications to ecology, pathology, and molecular medicine.

Recent advances in sequencing and functional metagenomic and metaproteomic profiling have elucidated the "blueprints" for cellular genetic, regulatory, and metabolic processes. These analyses comprise an emerging base that allows research to focus on a genome-based understanding and, through that understanding, predict how cellular systems and their metabolic processes shape the foundation of a biological system. Whereas previous efforts in biochemistry and structural biology have focused on determining the structure and function of individual cellular parts, we now need to develop methods to probe the cell's response to chemical and physical perturbations, to identify cell−cell differences, and to detect the presence of rare cells or rare cellular events in a population of many cells—all with sufficient spatial, temporal, and chemical resolution. This requires a noninvasive chemical imaging technology with spatial resolution at the scale of individual whole cells and subcells and temporal resolutions compatible with the rates of important chemical reactions in biological processes.

One logical next step in the development of IR spectromicroscopy is the improvement of imaging speed. This is required for

studying multiple subpopulations simultaneously within an isogenetic population and for developing a fundamental understanding of population-level diversity. Currently, even with the huge improvements in S/N from a synchrotron source, mapping large areas at high spatial resolution with the raster scanning technique can be extraordinarily time intensive. For example, imaging a 100 $\times$ 100 μm area with a 3-μm step size can take nearly 20 min. Using longer average measurement times to improve the S/N can easily increase the acquisition time to hours or days! Focal plane array (FPA) technology has increased the speed of image acquisition by multiplexing the acquisition of data, but low S/Ns have limited its applicability to living cell measurements. One possible solution is to couple the high brightness of synchrotron radiation with these new detectors, but achieving the expected advantage remains a challenge.[49] Presently, many of the over thirty synchrotron IR facilities worldwide are investigating this prospect. The IR ENvironmental Imaging (IRENI) Facility at the Synchrotron Radiation Center (SRC) at the University of Wisconsin Madison is the first FPA-based SR-FTIR system available to users (http://www.src.wisc.edu/ireni/). The technology is still in its infancy, but it offers exciting possibilities for rapidly unraveling biochemistry in living cells and tissues.

Another logical direction is to integrate the SR-FTIR technology with high-density microfluidic chips with plumbing networks.[50] This advance will enable the automatic and precise manipulation of fluids to provide the "just-right" aqueous dimensions for circumventing obfuscation by water absorption and to provide the accurate "on-demand" management of environmental conditions to study the chemistry of living cells. This will permit investigations of many important cellular systems in aqueous environments over long time periods, including harmful processes such as those underlying chronic bacterial infections or beneficial processes such as those enabling biofuel energy production by microbes.

ACKNOWLEDGMENT

This work was supported by the U.S. Department of Energy Office of Biological and Environmental Research's Structural Biology Program through contracts DE-AC02-05CH11231 and KP1501021 with Lawrence Berkeley National Laboratory. The Advanced Light Source is supported by the Director, Office of Science, Office of Basic Energy Sciences, of the U.S. Department of Energy under contract DE-AC02-05CH11231.

Hoi-Ying N. Holman is the Director of the Berkeley Synchrotron Infrared Structural Biology (BSISB) Program at the Advanced Light Source (ALS), the Head of Chemical Ecology in the Earth Sciences Division (ESD), and a Virtual Institute for Microbial Stress and Survival (VIMSS) Investigator. Holman's research focuses on the development and application of technology to study the chemistry of living cells by integrating spectroscopy, microscopy, and microfluidics. She received her Ph.D. in Environmental Chemistry and Chemical Engineering from University of California at Berkeley. Hans Bechtel is a Senior Scientific Engineering Associate at the ALS IR beamlines and has over 13 years of experience with spectroscopic methods and analysis. Bechtel received his Ph.D. in Physical Chemistry from Stanford University and was a postdoctoral researcher in the Spectroscopy Laboratory at the Massachusetts Institute of Technology. Zhao Hao is a Senior Scientific Engineering Associate at the Chemical Ecology and the ALS infrared beamlines. Hao's current research focuses on multimode imaging, plasmonic metamaterials, and spectroscopic analysis and modeling. Hao received his Ph.D. from the Institute of Physics, Chinese Academy of Sciences, was the recipient of the 2000−2001 STA Fellowship from Japan's Science and Technology Agency, and taught general physics at Florida State University while working at the National High Magnetic Field Laboratory before joining ALS. Michael Martin is the Deputy Leader of the Scientific Support Group at the ALS. Martin received his Ph.D. in Physics from the State University of New York at Stony Brook. All are currently at Lawrence Berkeley National Laboratory. Address correspondence to H.-Y. N. Holman at MS. 70A-3317L, Lawrence Berkeley National Laboratory, One Cyclotron Road, Berkeley, CA 94720; hyholman@lbl.gov.

REFERENCES

(1) Harrison, J. J.; Ceri, H.; Roper, N. J.; Badry, E. A.; Sproule, K. M.; Turner, R. J. *Microbiology* **2005**, *151*, 3181–3195.
(2) Lewis, K. *Nat. Rev. Microbiol.* **2007**, *5*, 48–56.
(3) Losick, R.; Desplan, C. *Science* **2008**, *320*, 65–68.
(4) Avery, S. V. *Nat. Rev. Microbiol.* **2006**, *4*, 577–587.
(5) Zalzman, M.; Falco, G.; Sharova, L. V.; Nishiyama, A.; Thomas, M.; Lee, S. L.; Stagg, C. A.; Hoang, H. G.; Yang, H. T.; Indig, F. E.; Wersto, R. P.; Ko, M. S. H. *Nature* **2010**, *464*, 858–866.
(6) Acar, M.; Mettetal, J. T.; van Oudenaarden, A. *Nat. Genet.* **2008**, *40*, 471–475.
(7) Parker, F. S. *Applications of Infrared, Raman, and Resonance Raman Spectroscopy in Biochemistry*; Plenum Press: New York & London, 1983.
(8) Jeffrey, G. A. *An introduction to hydrogen bonding*; Oxford University Press: New York, 1997.
(9) Blout, E. R.; Mellors, R. C. *Science* **1949**, *110*, 137–138.
(10) Barer, R.; Cole, A. R. H.; Thompson, H. W. *Nature* **1949**, *163*, 198–201.
(11) Wood, D. L. *Science* **1951**, *114*, 36–38.
(12) Woernley, D. L. *Cancer Res.* **1952**, *12*, 516–523.
(13) Stevenson, H. J.; Bolduan, O. E. *Science* **1952**, *116*, 111–113.
(14) Bhargava, R.; Levin, I. W. *Anal. Chem.* **2001**, *73*, 5157–5167.
(15) Salzer, R.; Siesler, H. W., Eds.; *Infrared and Raman Spectroscopic Imaging*; Wiley-VCH: Weinheim, 2009.
(16) Carr, G. L.; Reffner, J. A.; Williams, G. P. *Rev. Sci. Instrum.* **1995**, *66*, 1490–1492.
(17) Dumas, P.; Sockalingum, G. D.; Sule-Suso, J. *Trends Biotechnol.* **2007**, *25*, 40–44.
(18) Sham, T. K.; Rivers, M. L. *Applications of Synchrotron Radiation in Low-Temperature Geochemistry and Environmental Sciences* **2002**, *49*, 117–147.
(19) Levenson, E.; Lerch, P.; Martin, M. C. *Infrared Phys. Techn.* **2008**, *51*, 413–416.
(20) Holman, H. Y. N.; Bjornstad, K. A.; McNamara, M. P.; Martin, M. C.; McKinney, W. R.; Blakely, E. A. *J. Biomed. Opt.* **2002**, *7*, 417–424.
(21) Miller, L. M. In *Infrared and Raman Spectroscopic Imaging*; Salzer, R., Siesler, H. W., Eds.; Wiley-VCH: Weinheim, 2009, pp 510.
(22) Holman, H.-Y. N.; Martin, M. C. In *Adv. in Agronomy*; Sparks, D., Ed.; Elsevier: New York, 2006; Vol. 90, pp 79−127.
(23) Holman, H. Y. N.; Perry, D. L.; Martin, M. C.; Lamble, G. M.; McKinney, W. R.; Hunter-Cevera, J. C. *Geomicrobiol. J.* **1999**, *16*, 307–324.
(24) Holman, H. Y. N.; Nieman, K.; Sorensen, D. L.; Miller, C. D.; Martin, M. C.; Borch, T.; McKinney, W. R.; Sims, R. C. *Environ. Sci. Technol.* **2002**, *36*, 1276–1280.
(25) Jamin, N.; Dumas, P.; Moncuit, J.; Fridman, W. H.; Teillaud, J. L.; Carr, G. L.; Williams, G. P. *Proc. Natl. Acad. Sci. U.S.A.* **1998**, *95*, 4837–4840.
(26) Cameron, D. G.; Martin, A.; Mantsch, H. H. *Science* **1983**, *219*, 180–182.
(27) Goff, K. L.; Quaroni, L.; Wilson, K. E. *Analyst* **2009**, *134*, 2216–2219.
(28) Iwamoto, R.; Ohta, K. *Appl. Spectrosc.* **1984**, *38*, 359–365.
(29) Hutson, T. B.; Mitchell, M. L.; Keller, J. T.; Long, D. J.; Chang, M. J. W. *Anal. Biochem.* **1988**, *174*, 415–422.
(30) Suci, P. A.; Vrany, J. D.; Mittelman, M. W. *Biomaterials* **1998**, *19*, 327–339.
(31) Kuimova, M. K.; Chan, K. L. A.; Kazarian, S. G. *Appl. Spectrosc.* **2009**, *63*, 164–171.
(32) Holman, H.-Y. N.; Miles, R.; Hao, Z.; Wozei, E.; Anderson, L. M.; Yang, H. *Anal. Chem.* **2009**, *81*, 8564–8570.
(33) Nasse, M. J.; Ratti, S.; Giordano, M.; Hirschmugl, C. J. *Appl. Spectrosc.* **2009**, *63*, 1181–1186.
(34) Tobin, M. J.; Puskar, L.; Barber, R. L.; Harvey, E. C.; Heraud, P.; Wood, B. R.; Bambery, K. R.; Dillon, C. T.; Munro, L. K. *Vib. Spectrosc.* **2010**, *53*, 34–38.
(35) Birarda, G.; Grenci, G.; Businaro, L.; Marmiroli, B.; Pacor, S.; Vaccari, L. *Microelectron. Eng.* **2010**, *87*, 806–809.
(36) Stewart, P. S.; Franklin, M. J. *Nat. Rev. Microbiol.* **2008**, *6*, 199–210.
(37) Whiteley, M.; Bangera, M. G.; Bumgarner, R. E.; Parsek, M. R.; Teitzel, G. M.; Lory, S.; Greenberg, E. P. *Nature* **2001**, *413*, 860–864.
(38) Portugal, J.; Sanchezbaeza, F. J. *Biochem. J.* **1995**, *306*, 185–190.
(39) Costerton, J. W.; Irvin, R. T.; Cheng, K. J. *Annu. Rev. Microbiol.* **1981**, *35*, 299–324.
(40) Kolodkin-Gal, I.; Romero, D.; Cao, S.; Clardy, J.; Kolter, R.; Losick, R. *Science* **2010**, *328*, 627–629.

(41) Woutersen, S.; Bakker, H. J. *Nature* **1999**, *402*, 507–509.
(42) Cowan, M. L.; Bruner, B. D.; Huse, N.; Dwyer, J. R.; Chugh, B.; Nibbering, E. T. J.; Elsaesser, T.; Miller, R. J. D. *Nature* **2005**, *434*, 199–202.
(43) Mukhopadhyay, A.; Redding, A. M.; Joachimiak, M. P.; Arkin, A. P.; Borglin, S. E.; Dehal, P. S.; Chakraborty, R.; Geller, J. T.; Hazen, T. C.; He, Q.; Joyner, D. C.; Martin, V. J. J.; Wall, J. D.; Yang, Z. K.; Zhou, J.; Keasling, J. D. *J. Bacteriol.* **2007**, *189*, 5996–6010.
(44) Holman, H. Y. N.; Wozei, E.; Lin, Z.; Comolli, L. R.; Ball, D. A.; Borglin, S.; Fields, M. W.; Hazen, T. C.; Downing, K. H. *Proc. Natl. Acad. Sci. U.S.A.* **2009**, *106*, 12599–12604.
(45) Moss, D. A.; Keese, M.; Pepperkok, R. *Vib. Spectrosc.* **2005**, *38*, 185–191.
(46) Heraud, P.; Wood, B. R.; Tobin, M. J.; Beardall, J.; McNaughton, D. *Fems. Microbiol. Lett.* **2005**, *249*, 219–225.
(47) Jilkine, K.; Gough, K. M.; Julian, R.; Kaminskyj, S. G. W. *J. Inorg. Biochem.* **2008**, *102*, 540–546.
(48) Munro, K. L.; Bambery, K. R.; Carter, E. A.; Puskar, L.; Tobin, M. J.; Wood, B. R.; Dillon, C. T. *Vib. Spectrosc.* **2010**, *53*, 39–44.
(49) Petibois, C.; Piccinini, M.; Guidi, M. C.; Marcelli, A. *J. Synchrotron Radiat.* **2010**, *17*, 1–11.
(50) Thorsen, T.; Maerkl, S. J.; Quake, S. R. *Science* **2002**, *298*, 580–584.

AC100991D